Supporting Information

Morphology-Engineered Highly Active and Stable Ru/TiO_2 Catalysts for Selective CO Methanation

Shilong Chen,[a]+ *Ali M. Abdel-Mageed,*[a]+ *Dan Li,*[b] *Joachim Bansmann,*[a] *Sebastian Cisneros,*[a] *Johannes Biskupek,*[c] *Weixin Huang,*[b]* *R. Jürgen Behm*[a]*

[a] *Institute of Surface Chemistry and Catalysis, Ulm University, D-89069 Ulm, Germany*

[b] *Hefei National Laboratory for Physical Sciences at the Microscale, Key Laboratory of Surface and Interface Chemistry and Energy Catalysis of Anhui Higher Education Institutes and Department of Chemical Physics, University of Science and Technology of China, 230026 Hefei, China.*

[c] *Central Facility for Electron Microscopy, Group of Electron Microscopy of Materials Science, Ulm University, D-89069 Ulm, Germany*

*****Corresponding authors: W. Huang: huangwx@ustc.edu.cn and R.J. Behm: juergen.behm@uni-ulm.de

+ These authors contributed equally.

Experimental Section

Catalysts Preparation and Pre-treatment

Synthesis of TiO_2 NCs with different morphologies: Anatase TiO_2-{001} was prepared by a hydrothermal procedure.[1] Typically, 25 mL of the $Ti(OBu)_4$ precursor and 3 mL HF aqueous solution (40 wt.%) were mixed under stirring (250 rpm) at room temperature (RT). The solution was then transferred into a 50 mL Teflon lined stainless steel autoclave and kept at 180 °C for 24 h. The resulting white precipitate was collected by centrifugation, washed repeatedly with ethanol and water, and finally dried at 70 °C for 12 h. The dry powder was subsequently dispersed in 700 mL NaOH aqueous solution (0.1 mol/L), stirred for 24 h at RT, centrifuged, and washed repeatedly with water until the suspension pH value of aqueous solution was around 7.5.

Anatase TiO_2-{100} and TiO_2-{101} NCs were prepared following Liu et al.'s procedure.[2] Typically, 6.6 mL $TiCl_4$ salt solution (100%) was added drop-wisely into 20 mL HCl aqueous solution (0.43 mol/L) at 0 °C. After stirring for additional 30 min, the solution was added drop-wisely into 50 mL of NH_3 aqueous solution (5.5 wt.%) under continuous stirring at RT. Then the pH value of the solution was adjusted to between 6 and 7 using 4 wt.% NH_3 aqueous solution. The system was subsequently stirred at RT for 2 h. The resulting precipitate was filtered, washed repeatedly with water until the residual Cl^- was completely removed. The precipitated was then dried at 70 °C for 12 h to acquire $Ti(OH)_4$ precursor. To prepare anatase TiO_2-{100} NCs, 2.0 g $Ti(OH)_4$ and 0.5 g $(NH_4)_2SO_4$ salt were dispersed together in a mixture of 15 mL H_2O and 15 mL isopropanol under stirring at RT, then the mixture was transferred into a 50 mL Teflon-lined stainless steel autoclave and kept at 180 °C for 24 h. The resulting white precipitate was collected and washed repeatedly with water. To prepare anatase TiO_2-{101} NCs, 2.0 g $Ti(OH)_4$ and 0.2 g NH_4Cl salt were dispersed in a mixture of 15 mL H_2O and 15 mL isopropanol under stirring at RT, then the mixture was transferred into a 50 mL Teflon-lined stainless steel

autoclave and kept at 180 °C for 24 h. The resulting white precipitate was collected and washed repeatedly with water.

Preparation of Ru/TiO_2 catalysts: Ru/TiO_2 catalysts were prepared by incipient wetness impregnation.[3;4] Typically, 63.5 mg Ru precursor ($RuCl_3$ hydrate) was dissolved in 1.58 mL Millipore water before adding 1 g TiO_2 nanocrystals under continuously stirring for 1 h at low rotation rate (rpm = 250) to avoid inhomogeneous loading of the Ru precursor. Key point to produce highly dispersed and homogenously distributed Ru NPs is the precise control of the amount of water, which should comparable to the pore volume. The resulting Ru catalyst precursors were dried at 25°C overnight to remove any excess water.

Catalyst pretreatment and activation: Prior to all experiments, the catalyst precursors were pretreated *in situ* by calcination and subsequent reductive activation in the reaction gas atmosphere to acquire Ru/TiO_2 catalysts. During the calcination process, the catalyst precursor was heated to 150 °C within 10 min in a flow of N_2 (41.6 Nml min^{-1}), then the gas stream was switched to 10% O_2/N_2 (41.6 Nml min^{-1}) and kept for 30 min, and then the gas stream was switched back to N_2 (41.6 Nml min^{-1}) and kept for 15 min. During the subsequent reductive activation process, the gas stream was switched to the reaction gas atmosphere and the samples was heated from 150 °C to the reaction temperature (190 °C).

Characterization Methods

Ru loading and specific surface area: The Ru loadings of the catalysts were analyzed by inductively coupled plasma optical emission spectroscopy (ICP-OES). The BET specific surface area of the catalysts were measured by N_2 adsorption with using a Micromeritics Tristar II 3020M system.

Transmission Electron Microscopy (TEM): The Ru particle size and shape were determined from TEM micrographs taken after reaction for 10 min and 1000 min, respectively. The

particles were deposited by drop coating onto lacey carbon TEM grids (Plano GmbH). The TEM measurements were performed on a JEOL JEM-2100F operated at 200 kV and image side-aberration corrected FEI Titan operated at 300 kV. For detailed information on the Ru particle size (volume-area mean diameter and size distribution) and Ru particle shape (hemispherical or flat), at least 600 particles were evaluated for each sample. Assuming hemispherical Ru NPs and a surface density of 1.5×10^{15} Ru atoms cm^{-2}, the Ru dispersion was calculated from the volume-area mean diameter.

Dispersion of Ru nanoparticles: Calculation from TEM results: With the known diameter (d_i) of the individual of Ru nanoparticles (n_i), as measured by TEM, the volume-area mean diameter (d_{VA}) was calculated according to equation (1). From this relation one can easily calculate the Ru metal dispersion (D_{Ru}), which is defined by the ratio of surface atoms to the total number of atoms in the hemispherical metal particle (V_{Ru} = volume Ru atom, a_{Ru} = surface area Ru atom) as shown in equation (2).

$$d_{VA} = \frac{\sum_i n_i d_i^3}{\sum_i n_i d_i^2} \qquad (1)$$

$$D_{Ru} = 6 \frac{V_{Ru}/a_{Ru}}{d_{VA}} \qquad (2)$$

X-ray diffraction (XRD): XRD measurements of the Ru catalysts after reaction for 1000 min in SR-ref 6000 reformate were performed on a Siemens D5000 diffractometer, using Cu K_α line ($\lambda = 0.154$ nm).

X-ray photoelectron spectroscopy (XPS): XP spectra were recorded on a PHI 5800 ESCA system (Physical Electronics), using monochromatized Al K_α radiation (1486 eV). The pass energy for survey spectra was 93.9 eV, for detail spectra we used 29.35 eV. Spectra of the Ru catalysts were recorded after reaction. The binding energies (BEs) of all spectra were calibrated with respect to the C (1s) peak of ubiquitous carbon, which was fixed at a binding energy of 284.8 eV. The deconvolution of XP spectra was performed using a public XPS peak fitting

program (XPSPEAK4.1). A Shirley-type background was subtracted before the peak-fitting process, we assumed Lorentzian-Gaussian peak shapes with a Lorentzian contribution of about 20%.

Electron paramagnetic resonance (EPR): EPR spectra were recorded on a JEOL JES-FA200 EPR spectrometer (9.063 GHz, X-band) at 130 K with employed microwave power, modulation frequency and modulation amplitude of 0.998 mW, 100 kHz and 0.35 mT, respectively.

Kinetic Measurements

The activity experiments were performed in a fixed-bed quartz tube micro-reactor at atmospheric pressure in a continuous flow of H_2-rich reformate gases (SR-ref 6000: 6000 ppm CO, 3.0% N_2, 15.5% CO_2, H_2 balance and SR-ref 100: 100 ppm CO, 15.5% CO_2, 3% N_2 and H_2 balance), using high purity gases (Westfalen AG, purity ≥ 99.997%). The gas mixtures were prepared using mass flow controllers from Hastings (HFC-202), with a total gas flow of 41.6 Nml min^{-1}. To ensure differential reaction conditions (conversion < 20%), the catalysts were diluted with varying amounts of catalytically inactive and thermally stable α-Al_2O_3 (dilution 1:10 to 1:300, catalyst : α-Al_2O_3). In total, about 200 mg of the diluted catalyst was used, resulting in a catalyst bed length of ~1.2 cm. Partial pressures of the influent and effluent gases were analyzed by online gas chromatography with a CO detection limit of ca. 5 ppm (DANI 86.10), using thermal conductivity detectors (H_2 used as carrier gas). The Ru-mass-normalized reaction rate for CO methanation ($CO + 2H_2 \rightarrow CH_4 + H_2O$) was calculated from the CO conversion (X_{CO}) under differential reaction conditions (X_{CO} < 20%, see above), using the molar flow rate of CO into the reactor ($n_{CO,in}$), and the absolute mass of Ru metal (m_{Ru}) according to eq. 1. The Ru-mass-normalized CH_4 formation rate, in contrast, was calculated from the effluent molar flow rate of the CH_4 formed ($n_{CH4,out}$) (eq. 2). From these Ru-mass-normalized reaction rates, the molar mass of Ru (M_{Ru}) and the Ru dispersion (D_{Ru}) we

calculated the turnover frequencies (TOFs) according to eq. 3. The selectivity for CO methanation (S_{CO}) is given by the ratio of the CO methanation rate compared to that of the overall methane formation (from CO and CO_2, see eq. 4).

$$R_{\mathrm{CO}} = \frac{\mathrm{X_{CO}} \times \mathrm{n_{CO,in}}}{\mathrm{m_{Ru}}} \quad (1)$$

$$R_{\mathrm{CH_4}} = \frac{\mathrm{n_{CH_4,out}}}{\mathrm{m_{Ru}}} \quad (2)$$

$$\mathrm{TOF} = \frac{R_{\mathrm{CH_4}} \times \mathrm{M_{Ru}}}{\mathrm{D_{Ru}}} \quad (3)$$

$$S_{CO} = \frac{R_{\mathrm{CO}}}{R_{\mathrm{CH_4}}} = \frac{R_{\mathrm{CO}}}{R_{\mathrm{CO}} + R_{\mathrm{CO_2}}} \quad (4)$$

In situ diffuse reflectance FTIR spectroscopy (DRIFTS) Measurements

In situ DRIFTS measurements were performed on a Nicolet iS-50 FTIR spectrometer equipped with a *Harrick* reaction cell (HV-DR2) and using a MCT narrow band detector.[5] The catalyst bed was prepared by depositing about 70 mg of the diluted catalyst (1:10 with α-Al_2O_3) on a 100 mg α-Al_2O_3 layer, resulting in a total CO conversion of < 20%. The catalyst was pre-treated and activated in the same way described in kinetic measurements part. The intensities of adsorbed species were evaluated in Kubelka−Munk units (KMU), which are generally proportional to the concentration of respective surface adsorbates.[6;7] The total integrated intensities of all CO_{ad} related bands in the DRIFT spectra were determined by integrating the band area between 2170 and 1900 cm^{-1}. A DRIFTS spectrum of the fresh pre-treated catalyst purged with N_2 at 150 °C was taken as background.

Operando X-ray Absorption Spectroscopy (XAS)

Time resolved operando XAS measurements were performed at the energy-dispersive ID24 beamline at European Synchrotron Radiation Facility (ESRF), Grenoble. All XAS measurements were taken in transmission at Ru K-edge (22117 eV) using a Si (111)

polychromator in Laue configuration and utilizing a two-dimensional FReLoN CCD detector.[8] A specially designed reaction cell used in previous studies,[9-11] was used for the XAS measurements. 50 mg of Ru/TiO_2 diluted with □α-Al_2O_3 (2:1, roughly 33 mg Ru/TiO_2) was loaded in the reaction cell. Note that the amount of the catalyst is roughly 2 times larger than the amount used in the kinetics measurements to allow for the reasonable signal-to-noise ratio (for conversions, see Figure S1 – Supporting Information). The data acquisition took 10 s per spectrum. For the EXAFS spectra we averaged the spectra collected over 15 min. A Ru foil, a pellet of Ru(IV) oxide and $RuCl_3$, which were measured in transmission mode, were used as reference materials for the data evaluation. Background removal and spectra normalization as well as the linear combination analysis (LCA) of the XANES spectra were performed using the Athena software from the IFEFFIT program package.[12;13] The data reduction and subsequent fits of EXAFS spectra were carried out using the XDAP software package with standard procedures described elsewhere.[14] Theoretical references were calculated by FEFF 8.0 and calibrated with experimental references of Ru foil and RuO_2 powder.[15;16] The EXAFS data were evaluated in the R-space (R: 0.0 − 4.3 Å), using the k-range from 3.2 to 11.8 $Å^{-1}$. In the EXAFS data fit, we allowed the coordination number (CN), the Debye-Waller factor (DWF), the Ru-Ru bond length (R), and the energy shift (E_0) to change freely.

Calculation of the relative contributions of different facets in anatase TiO_2 nanocrystals

Based on the TEM results and assuming particle shapes expected from the Wulff shapes, we calculated the contributions from different facet orientations for the different types of TiO_2 nanocrystals through statistical analysis of TEM images.[17;18]

1. TiO_2-{001} nanocrystals

TiO_2-{001} nanocrystals exhibit two types of facets, with {001} and {101} orientation. This is illustrated in the geometrical model of a TiO_2-{001} nanocrystal presented below. Using the size values given below, which were derived from a statistical analysis of TiO_2 nanocrystals in TEM images, the fraction of the dominant {001} crystal plane is around 80%.

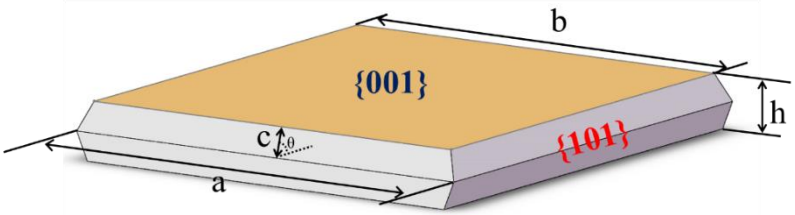

a = 55 nm

b = 52 nm

h = 6 nm

θ = 68.3°

$$c = \frac{h}{2 \times \sin\theta}$$

$$S_{001} = 2 \times b^2$$

$$S_{101} = 8 \times \frac{1}{2}(a+b) \times c$$

$$P_{001} = \frac{S_{001}}{S_{001} + S_{101}} = 80\%$$

$$P_{101} = \frac{S_{101}}{S_{001} + S_{101}} = 20\%$$

2. TiO_2-{100} nanocrystals

TiO_2-{100} nanocrystals exhibit three types of facets, with {100}, {001} and {101} orientation. This is illustrated in the geometrical model of a TiO_2-{100} nanocrystal presented below. Using the size values given below, which were derived from a statistical analysis of TiO_2 nanocrystals in TEM images, the fraction of the dominant {100} crystal plane is around 80%.

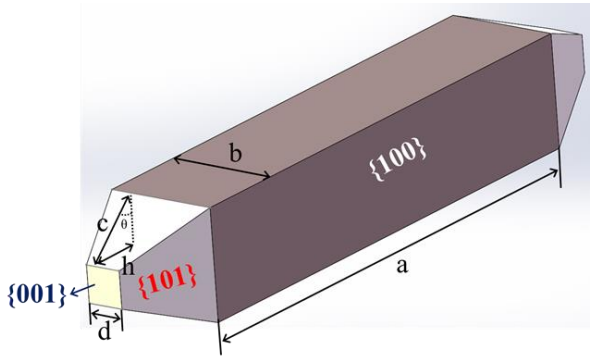

a = 50 nm
b = 14 nm
d = 4 nm
h = 11 nm
θ = 68.3°
$c = \frac{h}{\sin\theta}$

$$S_{001} = 2 \times d^2$$
$$S_{100} = 4 \times (a \times b)$$
$$S_{101} = 8 \times \frac{1}{2}(b + d) \times c$$
$$P_{001} = \frac{S_{001}}{S_{001} + S_{100} + S_{101}} = 1\%$$
$$P_{100} = \frac{S_{100}}{S_{001} + S_{100} + S_{101}} = 76\%$$
$$P_{101} = \frac{S_{101}}{S_{001} + S_{100} + S_{101}} = 23\%$$

3. TiO_2-{101} nanocrystals

TiO_2-{101} nanocrystals exhibit two types of facets, with {001} and {101} orientation. This is illustrated in the geometrical model of a TiO_2-{101} nanocrystal presented below. Using the size values given below, which were derived from a statistical analysis of TiO_2 nanocrystals in TEM images, the fraction of the dominant {101} crystal plane is almost 100%.

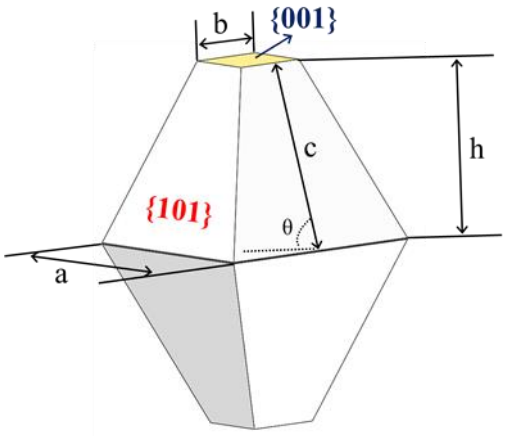

a = 13.5 nm

b = 3.5 nm

h = 12.5 nm

θ = 68.3°

$c = \frac{h}{\sin\theta}$

$S_{001} = 2 \times b^2$

$S_{101} = 8 \times \frac{1}{2}(a+b) \times c$

$P_{001} = \frac{S_{001}}{S_{001} + S_{101}} = 2\%$

$P_{101} = \frac{S_{101}}{S_{001} + S_{101}} = 98\%$

Table S1: BET specific surface area and Ru loading of the Ru/TiO_2 catalysts.

Catalyst	Surface area (m^2/g)	Ru loading (wt%)
Ru/TiO_2-{001}	102	1.94
Ru/TiO_2-{100}	99	1.91
Ru/TiO_2-{101}	108	1.99

Table S2: Structural parameters extracted from the evaluation of EXAFS spectra collected on the Ru/TiO_2-{001} catalyst during selective CO methanation in SR-ref 6000 reformate at 190°C.

Time	Scatterer	CN	DWF/ $Å^2$	R / Å	E_0 / eV
Calcined	Ru-O	1.30	-0.0082	2.150	-19.20
7	Ru-Ru	3.82	0.00408	2.628	14.15
	Ru-O	0.15	-0.01705	2.081	-6.50
23	Ru-Ru	3.50	0.00109	2.624	15.01
	Ru-O	0.23	-0.0169	2.065	-7.72
48	Ru-Ru	4.52	0.00645	2.628	14.75
	Ru-O	0.11	-0.0184	2.082	-10.95
64	Ru-Ru	4.45	0.00499	2.640	12.60
	Ru-O	0.11	-0.0244	2.102	-15.73
118	Ru-Ru	4.45	0.00342	2.654	12.05
	Ru-O	0.01	-0.04345	2.110	-20.00
125	Ru-Ru	4.75	0.00407	2.657	11.80
	Ru-O	0.02	-0.03510	2.100	-2.00
241	Ru-Ru	5.10	0.00423	2.653	13.00
	Ru-O	0.02	-0.03681	2.098	-20.0
267	Ru-Ru	5.16	0.00540	2.634	15.95
	Ru-O	0.01	-0.02444	2.110	-19.88
290	Ru-Ru	5.22	0.00557	2.638	14.24
	Ru-O	0.01	-0.02942	2.110	-20.00
385	Ru-Ru	5.04	0.004369	2.657	11.8
	Ru-O	0.04	-0.03474	2.103	-20.00
400	Ru-Ru	5.41	0.00520	2.655	11.76
	Ru-O	0.05	-0.03270	2.101	-20.00
440	Ru-Ru	6.61	0.00736	2.645	14.65
	Ru-O	0.01	-0.08500	2.086	-20.00

[a]Times: indicate the beginning of the data acquisition after starting the reaction (15 min for each data point).[b]CN: Ru-Ru and Ru-O first shell coordination number. [c]DWF: Debye-Waller-Factor. [d]R: Ru-Ru or Ru-O bond distance. [e]E0: energy reference parameter.

Table S3: Structural parameters extracted from the evaluation of EXAFS spectra collected on the Ru/TiO_2-{100} catalyst during selective CO methanation in SR-ref 6000 reformate at 190°C.

Time	Scatterer	CN	DWF/ $Å^2$	R / Å	E_0 / eV
Calcined	Ru-O	2.90	0.00082	2.110	-8.91
6	Ru-Ru	1.18	-0.00284	2.600	16.33
	Ru-O	1.09	-0.00513	2.050	-0.06
25	Ru-Ru	2.10	-0.00206	2.613	17.93
	Ru-O	1.10	-0.00456	2.069	-6.50
45	Ru-Ru	3.70	0.00391	2.630	13.94
	Ru-O	0.31	-0.01278	2.077	-7.79
60	Ru-Ru	3.69	0.00632	2.641	12.50
	Ru-O	0.08	-0.001787	2.042	1.30
120	Ru-Ru	4.01	0.00792	2.643	12.49
	Ru-O	0.08	-0.01889	2.046	-1.32
135	Ru-Ru	4.30	0.0093	2.644	14.56
	Ru-O	0.07	-0.01981	2.071	2.70
260	Ru-Ru	4.02	0.00575	2.641	14.37
	Ru-O	0.013	-0.01632	2.055	-1.84
280	Ru-Ru	4.05	0.00533	2.641	14.36
	Ru-O	0.14	-0.01595	2.048	-0.45
330	Ru-Ru	4.17	0.00639	2.645	13.54
	Ru-O	0.18	-0.0217	2.033	-1.62
390	Ru-Ru	3.66	0.00420	2.641	12.47
	Ru-O	0.03	-0.02628	2.033	-16.12
420	Ru-Ru	3.88	0.00527	2.641	13.92
	Ru-O	0.05	-0.01933	2.034	-1.40
450	Ru-Ru	3.60	0.00354	2.649	12.99
	Ru-O	0.05	-0.01908	2.027	2.43

[a]Times: indicate the beginning of the data acquisition after starting the reaction (15 min for each data point).[b]CN: Ru-Ru and Ru-O first shell coordination number. [c]DWF: Debye-Waller-Factor. [d]R: Ru-Ru or Ru-O bond distance. [e]E0: energy reference parameter.

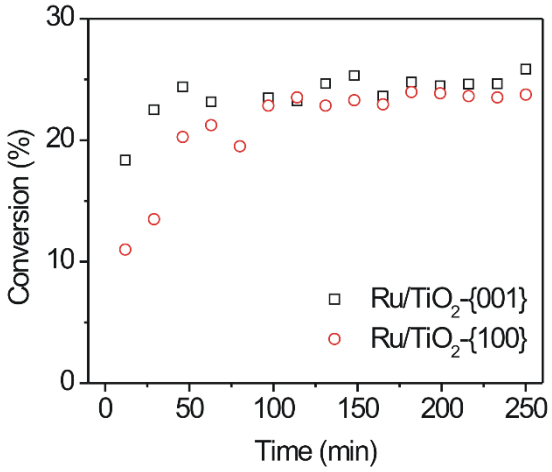

Figure S1: CO conversion for CO methanation in SR-ref 6000 reformate gas at 190 °C catalyzed by Ru/TiO_2 catalysts in the XAFS cell during the XAS measurements. (The used catalyst weight was 21 mg and 18 mg for Ru/TiO_2-{001} and Ru/TiO_2-{100}, respectively.) Reaction rates were not calculated due to the high CO conversion (CH_4 formation), which results in non-differential reaction conditions.

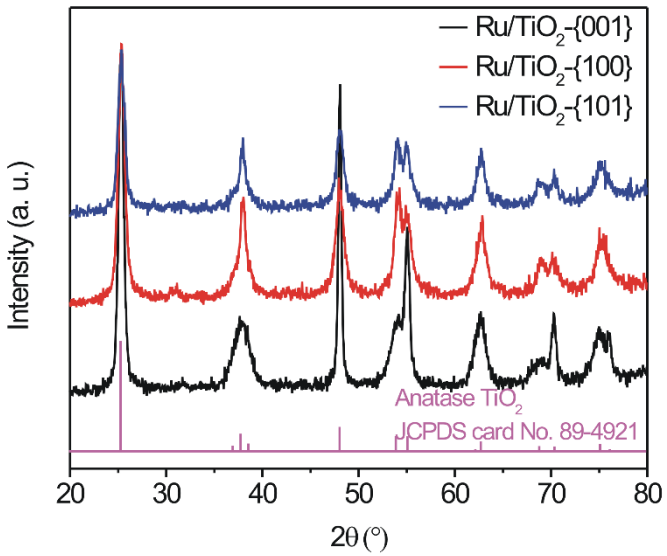

Figure S2: XRD diffractograms of Ru/TiO_2-{001}, Ru/TiO_2-{100}, and Ru/TiO_2-{101}. The typical pattern for the respective oxide phases TiO_2 anatase are shown.

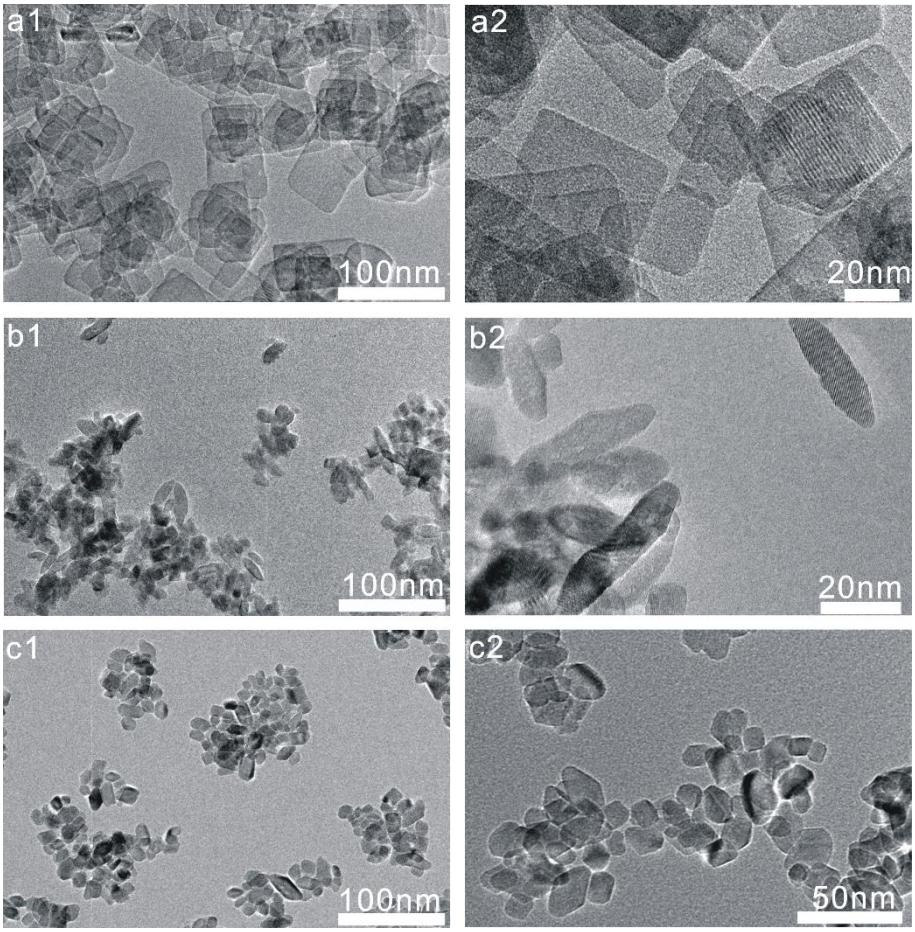

Figure S3: TEM images of as-synthesized TiO_2-{001} (a1 and a2), TiO_2-{100} (b1 and b2), and TiO_2-{101}(c1 and c2) nanocrystals.

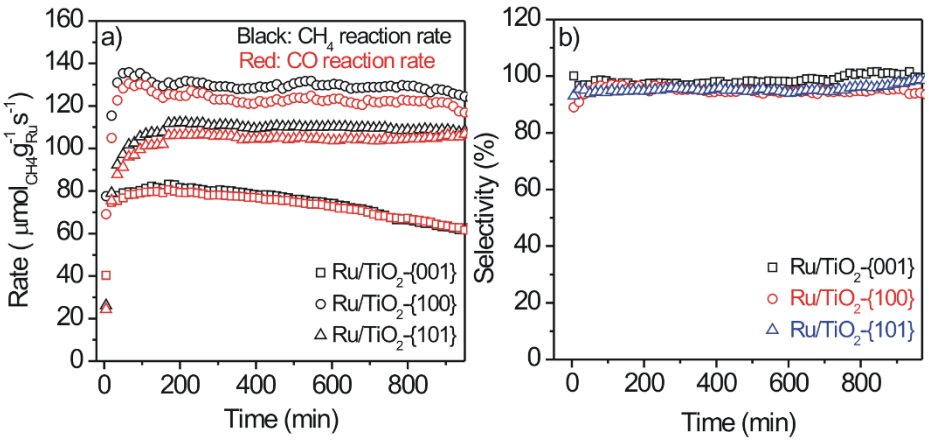

Figure S4: Temporal evolution of the Ru mass-normalized reaction rate (CH_4 formation and CO methanation) (a) and selectivity (b) for CO methanation during reaction in SR-ref 100 at 190 °C.

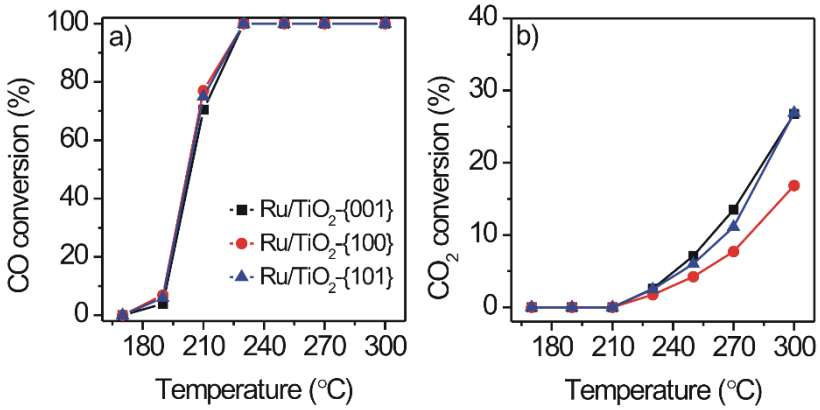

Figure S5: CO (a) and CO_2 (b) conversion during reaction in SR-ref 6000 in the temperature range from 170 to 300 °C.

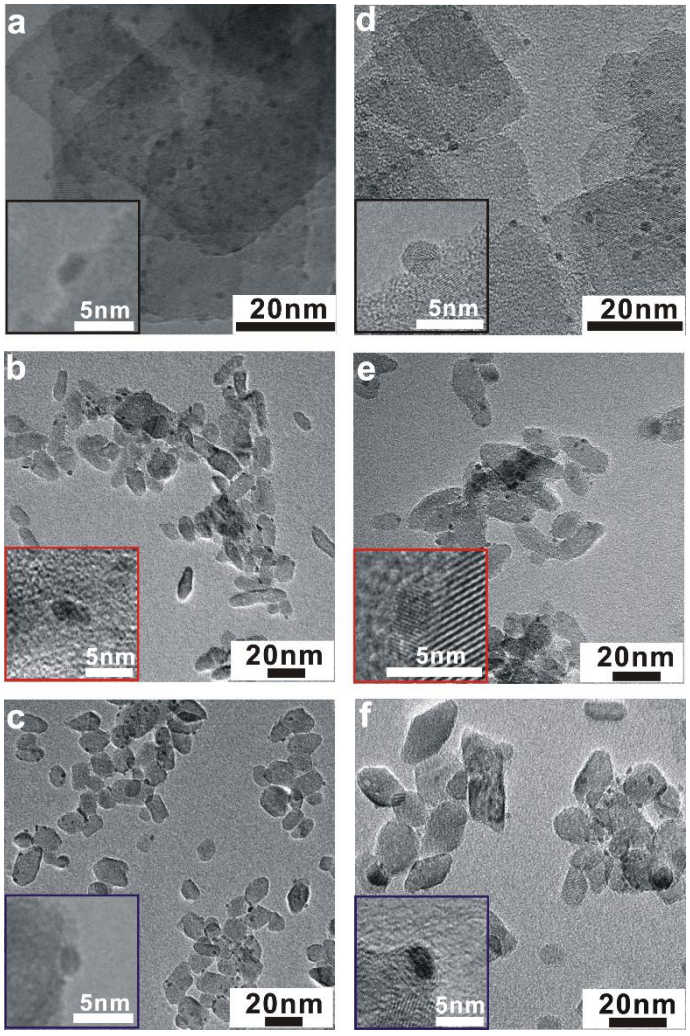

Figure S6: TEM images of Ru/TiO_2-{001} (a and d), Ru/TiO_2-{100} (b and e), and Ru/TiO_2-{101} (c and f) after reaction for 10 min (a-c) and 1000 min (d-f) in SR-ref 6000 at 190 °C, respectively, additional TEM images of each Ru/TiO_2 catalyst will be shown below in Figure S5-S7.

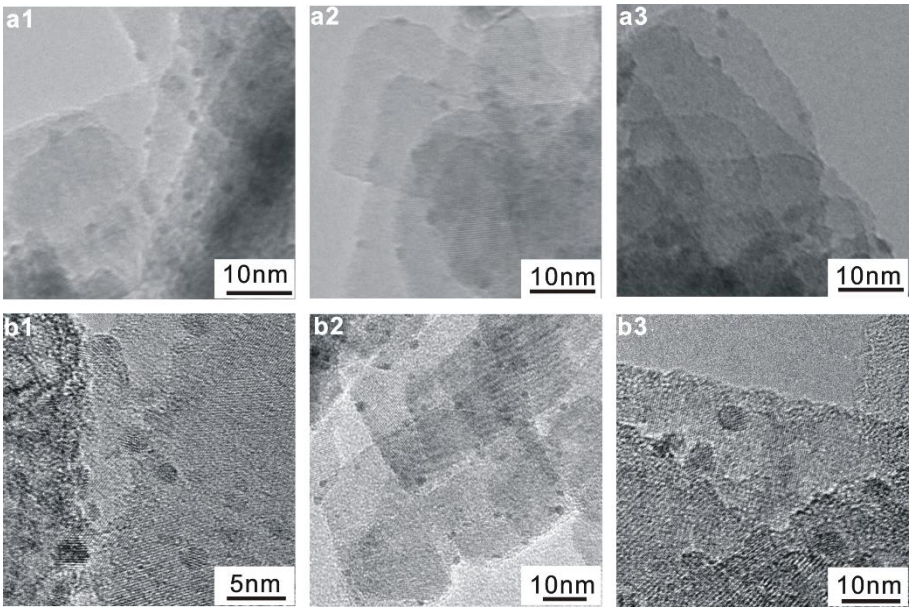

Figure S7: TEM images of Ru/TiO_2-{001} after reaction for 10 min (a1-a3) and 1000 min (b1-b3) in SR-ref 6000 at 190 °C, respectively.

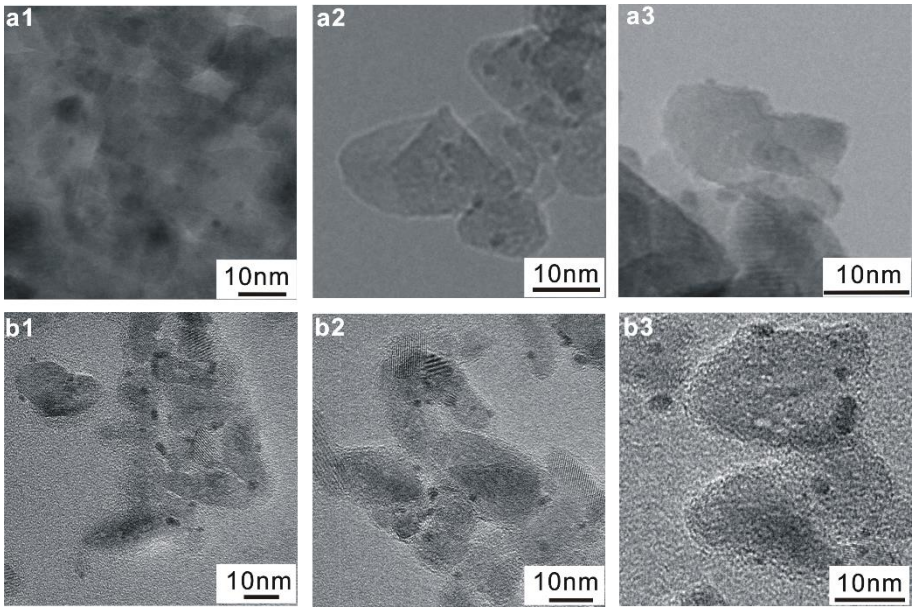

Figure S8: TEM images of Ru/TiO_2-{100} after reaction for 10 min (a1-a3) and 1000 min (b1-b3) in SR-ref 6000 at 190 °C, respectively.

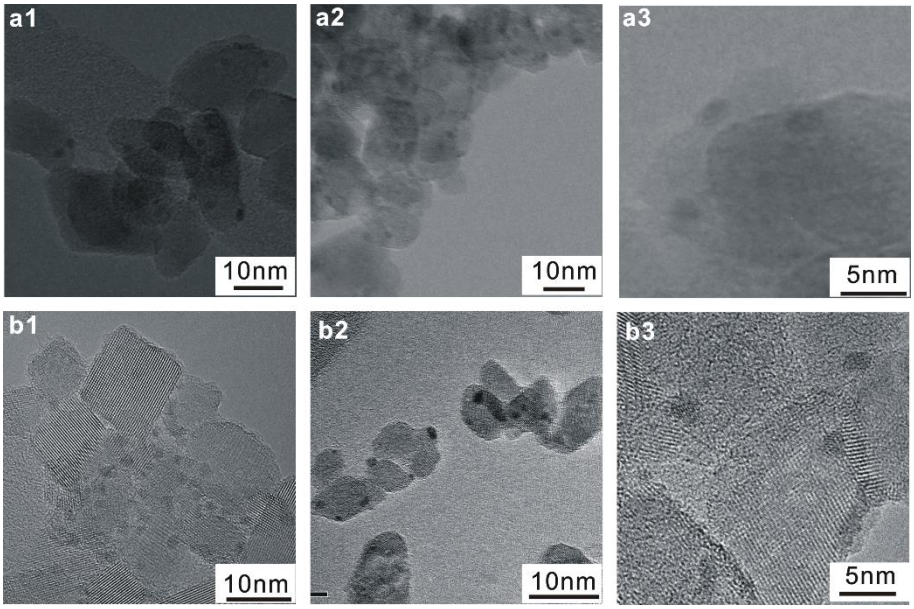

Figure S9: TEM images of Ru/TiO_2-{101} after reaction for 10 min (a1-a3) and 1000 min (b1-b3) in SR-ref 6000 at 190 °C, respectively.

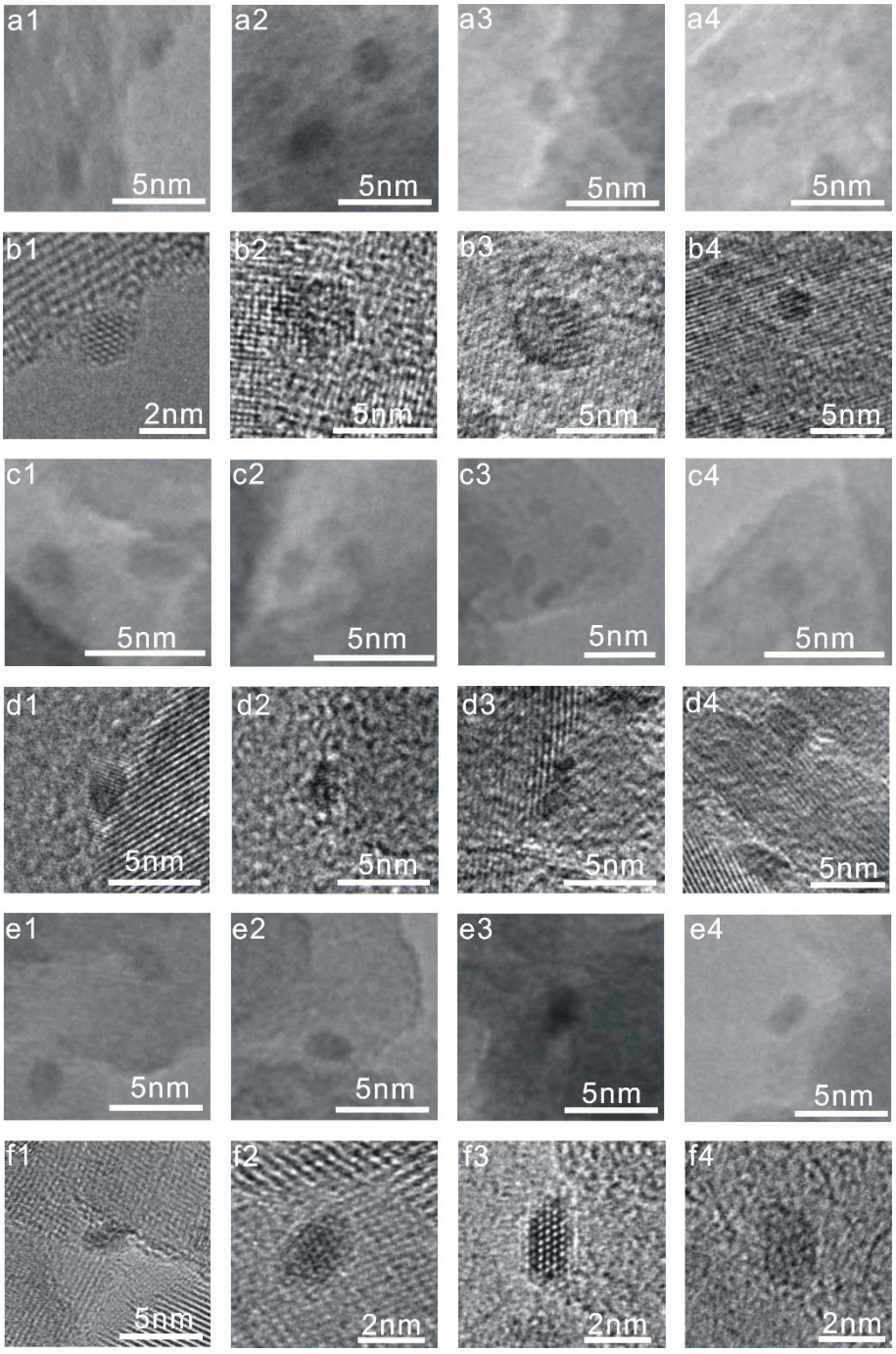

Figure S10: HR-TEM images of Ru/TiO_2-{001} (a, b), Ru/TiO_2-{100} (c, d), and Ru/TiO_2-{101} (e, f) after reaction for 10 min (a, c, e) and for 1000 min (b, d, f) in SR-ref 6000 at 190 °C, respectively.

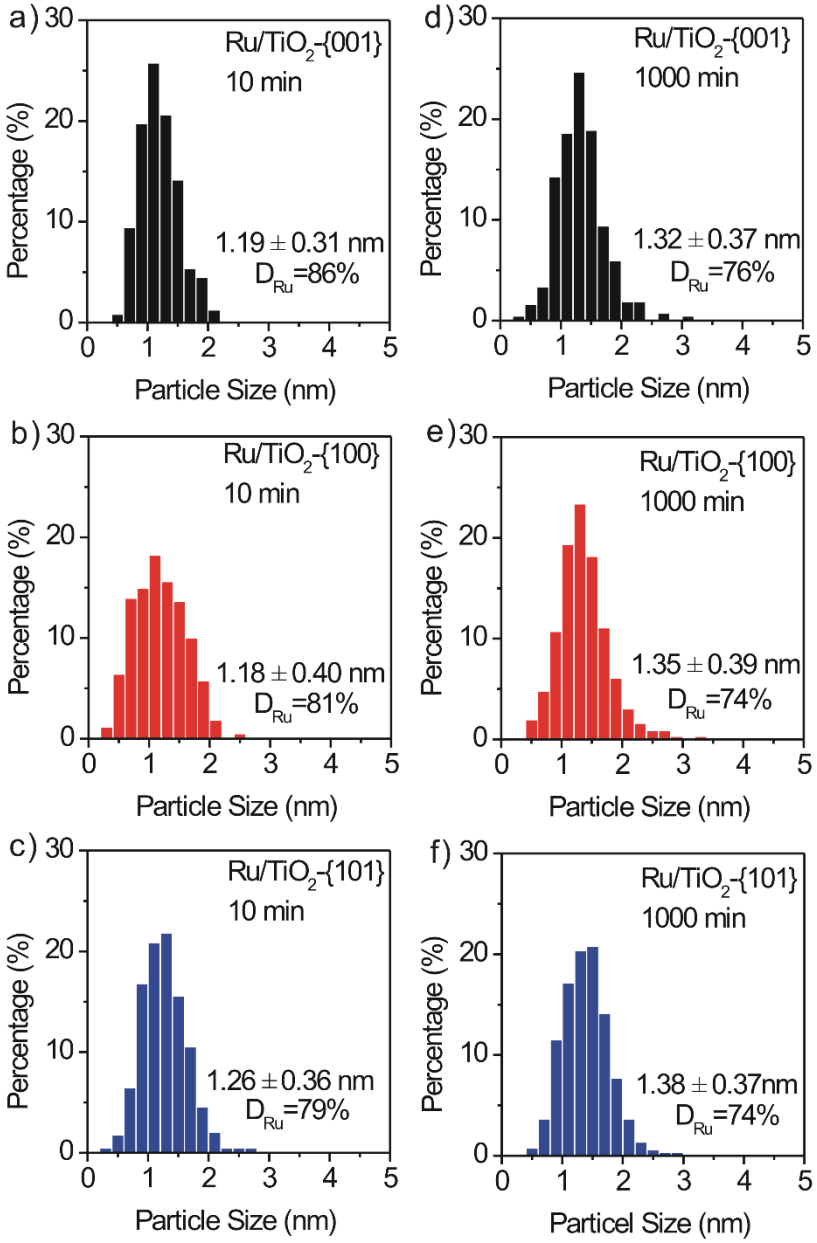

Figure S11: Ru particle size distributions of (a, d) Ru/TiO_2-{001}, (b, e) Ru/TiO_2-{100}, (c, f) Ru/TiO_2-{101} catalysts after reaction for 10 min (left panels: a, b, c) and 1000 min (right panels: d, e, f) in SR-ref 6000 gas mixture at 190 °C, respectively.

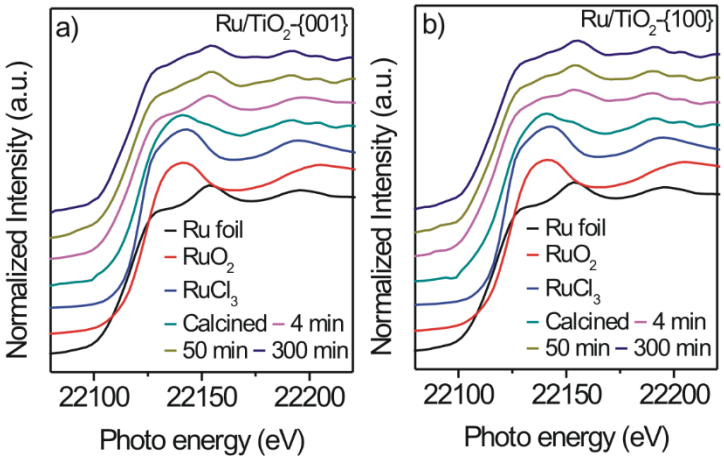

Figure S12: XANES spectra of references: Ru foil, RuO_2, $RuCl_3$ powder and (a) Ru/TiO_2-{001} and (b) Ru/TiO_2-{100} catalysts in N_2 at 150 °C after calcination in 10%O_2/N_2, and during reaction in SR-ref 6000 reformate at 190 °C at different reaction times: 4, 50, 300 min.

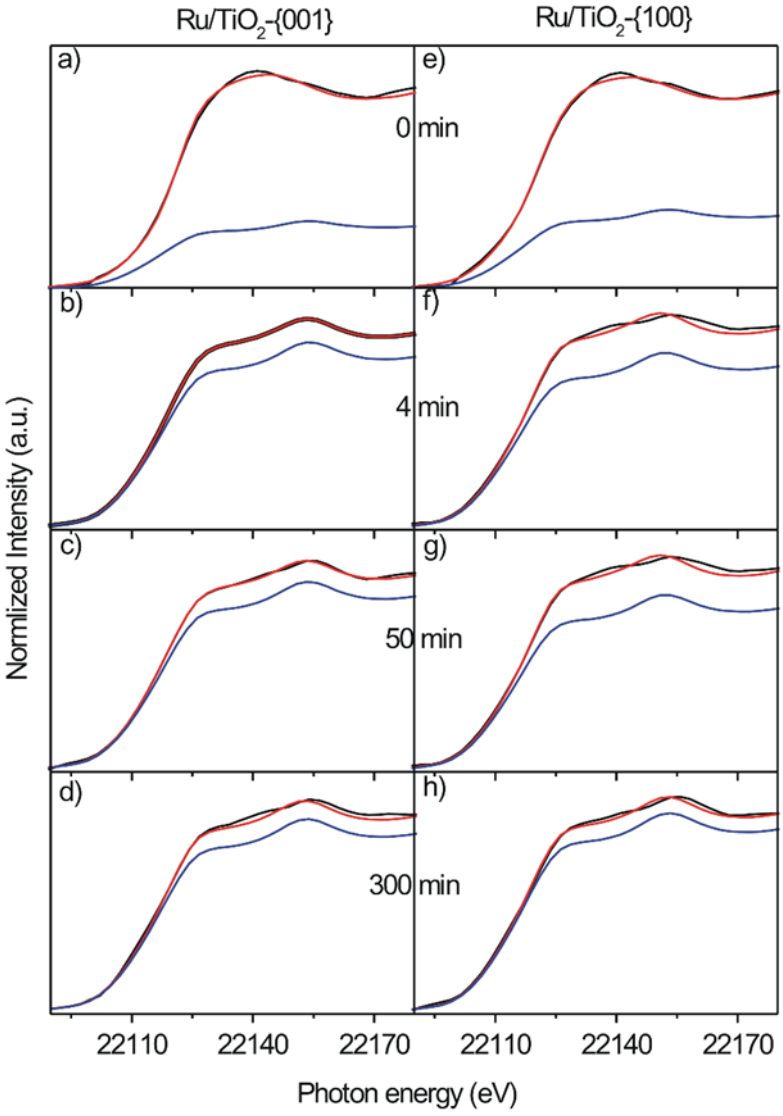

Figure S13: Linear combination analysis of selected Ru K-edge XANES spectra at different reaction times of (a-d) Ru/TiO_2-{001} and (e-h) Ru/TiO_2-{100} during reaction in SR-ref 6000 at 190 °C. Black lines: original spectra, red lines: fit curves based on a linear combination of Ru references (Ru foil, RuO_2 and $RuCl_3$ powder), blue lines: metallic Ru species contribution. 0 min refers to the catalyst in N_2 at 150°C after calcination.

As shown in Figure S10 a and e, the XANES spectra of Ru/TiO_2-{001} and Ru/TiO_2-{100} after calcination at 150 °C show a strong white line contribution (broad peak between 22120-22160 eV), whose feature is close to RuO_2 and / or $RuCl_3$. Upon switching to the reaction gas,

the white line intensity of both samples decreased dramatically at around 4 min (Figure S10 b and f), hinting at a fast reduction of the majority of oxidic Ru species; however, during the extended reaction times between 5 and 300 min, the XANES spectra of Ru/TiO_2-{001} and Ru/TiO_2-{100} evolve in different ways (Figure S10 c - g).

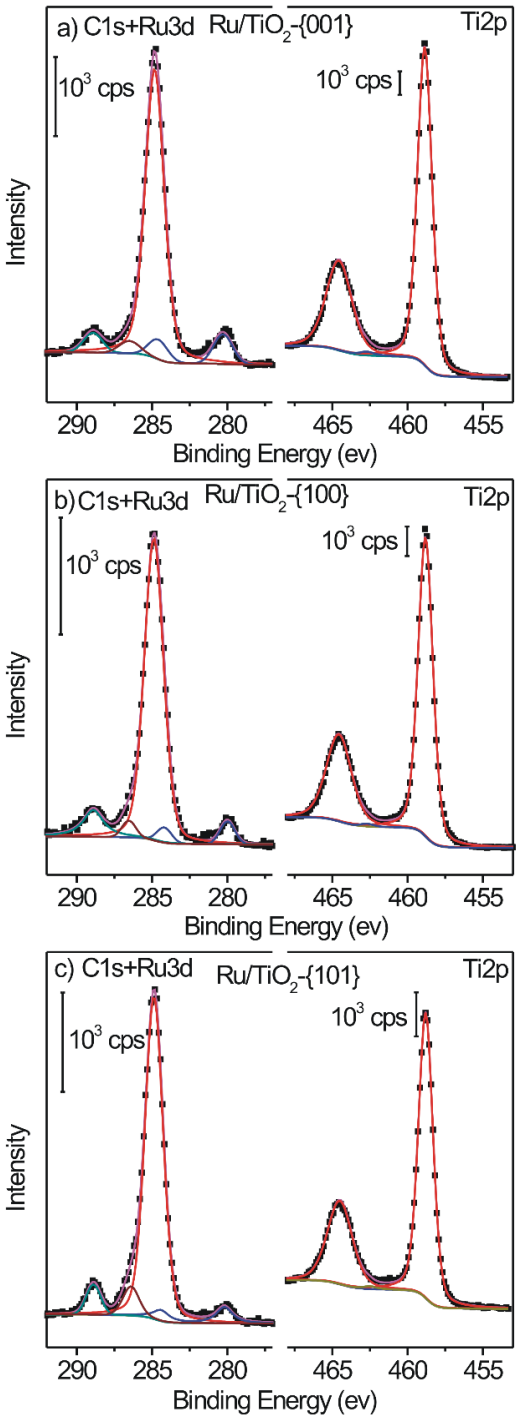

Figure S14: XP spectra of Ru 3d / C 1s and Ru 3p / Ti 2p regions of (a) Ru/TiO_2-{001}, (b) Ru/TiO_2-{100}, and (c) Ru/TiO_2-{101} after reaction for 1000 min in SR-ref 6000 gas reformate.

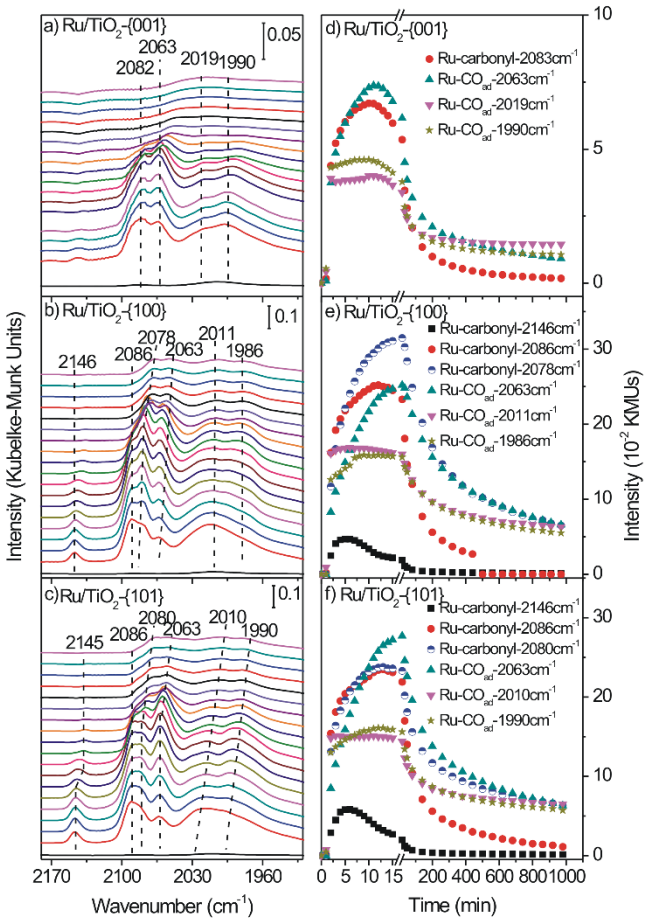

Figure S15: Time-resolved *in situ* DRIFT spectra recorded at different times during the selective CO methanation, and time evolution of the vibrational peak intensities (peak heights) of adsorbed CO surface species (see bands in the figure) on the (a, d) Ru/TiO_2-{001}, (b, e) Ru/TiO_2-{100}, and (c, f) Ru/TiO_2-{101} catalysts in SR-ref 6000 gas mixture at 190 °C (from bottom to top: 1, 3, 5, 7, 9, 11, 13, 15, 20, 35, 50, 80, 140, 260, 380, 500, 620, 740, 860, 970 min, respectively).

Ru/TiO_2-{001} initially exhibit vibrational bands for Ru-multicarbonyl at 2083 cm^{-1} and for CO_{ad} and at 2063, 2019 and 1990 cm^{-1} that reach a maximum coverage at around 10 min and then decayed fast with the reaction time. Ru/TiO_2-{100} and Ru/TiO_2-{101} initially show vibrational bands for Ru-multicarbonyl at 2146, 2086 and 2080 cm^{-1} and for CO_{ad} and at 2063, 2011 and 1986 cm^{-1}. It takes longer time for CO_{ad} on Ru/TiO_2-{100} and Ru/TiO_2-{101} to

reach the coverage maxima than on Ru/TiO_2-{001}, which can be related to the longer activation period of Ru/TiO_2-{100} and Ru/TiO_2-{101}. The CO_{ad} coverages on Ru/TiO_2-{100} and Ru/TiO_2-{101} also decay after the reach of the maxima, but they are much higher than those on Ru/TiO_2-{001}.

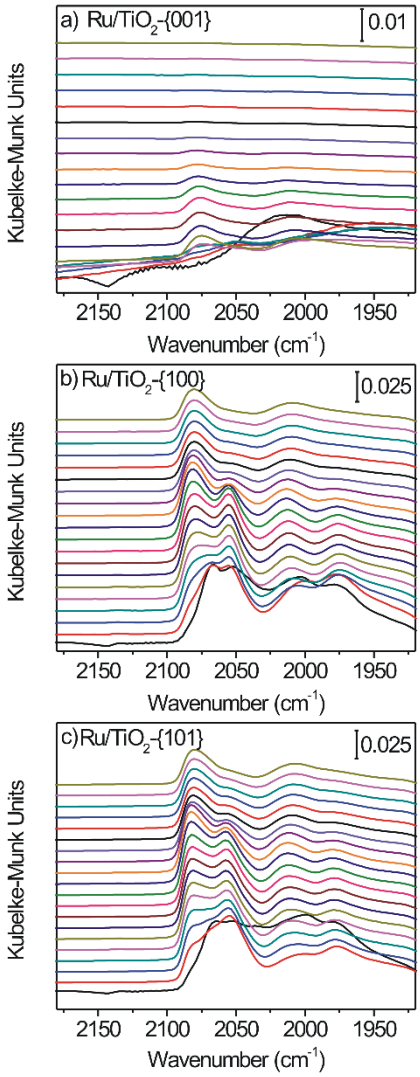

Figure S16: Representative DRIFT spectra recorded during isothermal N_2 desorption from (a) Ru/TiO_2-{001}, (b) Ru/TiO_2-{100}, and (c) Ru/TiO_2-{101} catalysts after 1000 min reaction in SR-ref 6000 gas mixture at 190 °C, from bottom to top: 0, 2, 4, 6, 8, 10, 12, 14, 15, 20, 35, 50, 80, 200, 320, 440, 560, 680, 800, 970 min.

References

[1] X. Han, Q. Kuang, M. Jin, Z. Xie, L. Zheng, *J. Am. Chem. Soc.* **2009**, *131,* 3152-3153.

[2] L. Liu, X. Gu, Z. Ji, W. Zou, C. Tang, F. Gao, L. Dong, *J. Phys. Chem. C* **2013**, *117,* 18578-18587.

[3] A. M. Abdel-Mageed, D. Widmann, S. E. Olesen, I. Chorkendorff, J. Biskupek, R. J. Behm, *ACS Catal.* **2015**, *5*, 6753-6763.

[4] S. Chen, A. M. Abdel-Mageed, C. Gauckler, S. E. Olesen, I. Chorkendorff, R. J. Behm, *J. Catal.* **2019**, *373*, 103-115.

[5] M. M. Schubert, T. P. Häring, G. Bräth, H. A. Gasteiger, R. J. Behm, *Appl. Spectrosc.* ***2*001**, *55*, 1537-1543.

[6] I. M. Hamadeh, P. R. Griffiths, *Appl.Spectrosc.* **1987**, *41*, *6*82-688.

[7] J. Sirita, S. Phanichphant, F. C. Meunier, *Anal.Chem.* ***2*007**, *79*, *3*912-3918.

[8] S. Pascarelli, O. Mathon, T. Mairs, I. Kantor, G. Agostini, C. Strohm, S. Pasternak, F. Perrin, G. Berruyer, P. Chappelet, C. Clavel, M. C. Dominguez, *J. Synchrotron Rad.* **2016**, *23*, *3*53-368.

[9] S. Eckle, M. Augustin, H.-G. Anfang, R. J. Behm, *Catal. Today* ***2*012**, *181,* 40-51.

[10] A. M. Abdel-Mageed, S. Eckle, H.-G. Anfang, R. J. Behm, *J. Catal.* **2013**, *298,* 148-160.

[11] A. M. Abdel-Mageed, G. Kucèrová J. Bansmann, R. J. Behm, *ACS Catal.* **2017***, 17*, 6471-6484.

[12] M. Newville, *J.Synchrotron Rad.* **2001**, *8*, 322-324.

[13] B. Ravel, M. A. T. H. Newville, *J.* S*ynchrotron Rad.* **2001**, *8*, 3*22*-324.

[14] M. Vaarkamp, J. C. Linders, D. C. Koningsberger, *Physica B* **1995***, 208-209,* 159-160.

[15] A. L. Ankudinov, B. Ravel, J. J. Rehr, S. D. Conradson, *Phys. Rev. B* **1998***, 58*, **7**565-7576.

[16] D. C. Koningsberger, B. L. Mojet, G. E. van Dorssen, D. E. Ramaker, *Top.* C*atal.* **2000***, 10,* 143-155.

[17] D. Li, R. You, M. Yang, Y. Liu, K. Qian, S. Chen, T. Cao, Z. Zhang, J. Tian, W. Huang, J. Phys. Chem. C **2019**, *123*, 10367-10376.

[18] L. Liu, X. Gu, Y. Cao, X. Yao, L. Zhang, C. Tang, F. Gao, L. Dong, *ACS Catal.* **2013**, 3, 2768-2775.